Available online at www.sciencedirect.com
SCIENCE DIRECT®
Remote Sensing of Environment 89 (2004) 351–360
Remote Sensing of Environment
www.elsevier.com/locate/rse

# Estimating fractional snow cover from MODIS using the normalized difference snow index

V.V. Salomonson[a,*], I. Appel[b]

[a] Earth Sciences Directorate, NASA/Goddard Space Flight Center, Mail Code 974, Greenbelt, MD 20771, USA
[b] Raytheon ITSS, 1616 McCormick Drive, Upper Marlboro, MD 20774, USA

Received 9 April 2003; received in revised form 14 September 2003; accepted 28 October 2003

**Abstract**

Snow-cover information is important for a wide variety of scientific studies, water supply and management applications. The NASA Earth Observing System (EOS) Moderate Resolution Imaging Spectroradiometer (MODIS) provides improved capabilities to observe snow cover from space and has been successfully using a normalized difference snow index (NDSI), along with threshold tests, to provide global, automated binary maps of snow cover. The NDSI is a spectral band ratio that takes advantage of the spectral differences of snow in short-wave infrared and visible MODIS spectral bands to identify snow versus other features in a scene. This study has evaluated whether there is a "signal" in the NDSI that could be used to estimate the fraction of snow within a 500 m MODIS pixel and thereby enhance the use of the NDSI approach in monitoring snow cover. Using Landsat 30-m observations as "ground truth," the percentage of snow cover was calculated for 500-m cells. Then a regression relationship between 500-m NDSI observations and fractional snow cover was developed over three different snow-covered regions and tested over other areas. The overall results indicate that the relationship between fractional snow cover and NDSI is reasonably robust when applied locally and over large areas like North America. The relationship offers advantages relative to other published fractional snow cover algorithms developed for global-scale use with MODIS. This study indicates that the fraction of snow cover within a MODIS pixel using this approach can be provided with a mean absolute error less than 0.1 over the range from 0.0 to 1.0 in fractional snow cover.


*Keywords:* MODIS; Fractional snow cover; Remote sensing; EOS Terra; EOS aqua

## 1. Introduction

The distribution of snow in space and time is an important parameter for a wide variety of reasons. Knowing the extent of the snow is valuable information in that it provides insight as to the amount of water to be expected from snowmelt available for runoff and water supply. In addition, the snow cover itself is a surface condition that affects radiation and water balance determinations that are inputs to hydrological cycle and climate studies (see, for examples, Cess et al., 1991; Cohen, 1994; Cohen & Entekhabi, 2001; Douville & Royer, 1996; Foster et al., 1996; Stieglitz, Ducharne, Koster, & Suarez, 2001; Yang et al., 1999). Furthermore, the sub-grid variability of snow within numerical models of hydrological or atmospheric surface energy exchange processes calls for knowing the fractional snow cover and its distribution as accurately as possible (see, for examples, Liston, 1995, 1999; Liston, Pielke, & Greene, 1999; Roesch, Wild, Gilgen, Ohmura, & Arugnell, 2001). Given the importance of knowing the distribution of snow, there has been much progress since 1966 when the first operational snow mapping was done by NOAA, in utilizing spaceborne sensors that provide daily, global observations to monitor the variability in space and time in the extent of snow cover (Frei & Robinson, 1998; Rango, Walker, & Goodison, 2000; Robinson, Dewey, & Heim, 1993).

The intent and purpose of this study was to examine whether estimates of fractional snow cover from the NASA Earth Observing System (EOS) Moderate Resolution Imaging Spectroradiometer (MODIS) could be improved by using the variability in the Normalized Difference Snow Index (NDSI) spectral band ratio to estimate the fraction of snow cover being observed in each MODIS pixel and subsequently offer some increased information regarding the presence

* Corresponding author. Tel.: +1-301-614-5631; fax: +1-301-614-5808.
*E-mail address:* Vincent.V.Salomonson@nasa.gov (V.V. Salomonson).

0034-4257/$ - see front matter © 2003 Elsevier Inc. All rights reserved.
doi:10.1016/j.rse.2003.10.016

of snow cover beyond that inherent with the basic MODIS pixel dimensions. In other words, rather than simply saying a MODIS pixel is either snow covered or not, there would be an estimate made as to the fraction of snow in each MODIS pixel based on the magnitude of the NDSI. This approach was pursued to see how much improvement might be offered by using the NDSI while retaining the computational simplicity inherent in the use of a rationing algorithm for automated processing of MODIS data to obtain daily, global estimates of snow-cover distribution.

## 2. Background

The MODIS instrument is a multispectral instrument with 36 bands and nominal spatial resolution of 250 m in 2 bands, 500 m in 5 bands, and 1 km in 29 bands. The MODIS instrument is operational on two EOS spacecraft. The Terra mission was launched with a MODIS instrument on it in December 1999 and observations provided from February 24, 2000, to the present. The Aqua mission was launched in May of 2002 and observations provided from June 24, 2002 to the present. The characteristics and specifications of the MODIS instrument are described by Barnes, Pagano, and Salomonson (1998) and the recent, general status of the instrument provided by Guenther, Xiong, Salomonson, Barnes, and Young (2002).

Relative to similar sensors such as the Advanced Very High Resolution Radiometer (AVHRR) that has been operational for many years on the NOAA Polar Operational Environmental Satellite System (POESS) the MODIS sensor offers some significant advantages. In the context of this study, the MODIS provides observations at a nominal spatial resolution of 500-m versus the 1.1-km spatial resolution of the AVHRR and continuously available (spatially and temporally), spectral band observations that span the visible and short-wave infrared wavelengths useful for distinguishing the extent of snow cover.

Hall, Riggs, and Salomonson (1995, Hall et al., 2002) and Klein, Hall, and Riggs (1998) have used the spectral differences in snow versus non-snow-covered areas that can be observed by the MODIS to develop an automated approach to providing daily, global observations of snow cover. The approach employs the NDSI that essentially takes advantage of the fact that snow reflectance is high in the visible (0.5–0.7 μm) wavelengths and has low reflectance in the short-wave infrared (1–4 μm) wavelengths (Nolin & Liang, 2000) to enable distinguishing snow from clouds and other non-snow-covered conditions. The NDSI is defined as the difference of reflectances observed in a visible band such as MODIS band 4 (0.555 μm) and a short-wave infrared band such as MODIS band 6 (1.640 μm) divided by the sum of the two reflectances:

$$\mathrm{NDSI} = (b4 - b6)/(b4 + b6). \quad (1)$$

The NDSI not only takes advantage of the spectral differences of snow versus non-snow-covered area and clouds, but also like many ratio approaches, tends to reduce (but certainly not totally eliminate) the influence of atmospheric effects and viewing geometry. An approach, called "SNOWMAP," is now being employed in an automated fashion to routinely provide global, snow-cover products for use by the hydrological science and water resource management communities (Hall et al., 2002). These products provide a determination that designates each MODIS pixel as either snow covered or not covered by snow. SNOWMAP includes the use of not only NDSI, but also other criteria to minimize false snow detection associated with lakes, or beaches, and adjustments for snow in forested areas versus non-forested areas. All the criteria, etc. are found in the MODIS Snow Products User Guide (http://modis-snow-ice.gsfc.nasa.gov/sug.pdf). For areas larger than a MODIS pixel such as the grid (e.g., 5 × 5 km) of a numerical model utilizing MODIS observations of snow cover, the fraction of snow cover in the grid simply takes the percentage of snow-covered pixels as a fraction of the total cloud-free, MODIS observations in the grid.

There is a need to enhance the utility of the MODIS snow-cover observations by providing information about the fraction of snow cover within a MODIS pixel. This is particularly true when trying to study snow processes in more localized areas associated with small watersheds, for example. There are several remote sensing approaches that have been applied for estimating the fractional snow cover within a sensor pixel (Nolin, Dozier, & Mertes, 1993; Painter, Dozier, Roberts, Davis, & Green, 2003; Rosenthal and Dozier, 1996; Vikhamer & Solberg, 2002). Recently Kaufman, Kleidman, Hall, Martins, and Barton (2002) and Barton, Hall, and Riggs (2001) have described some approaches for estimating subpixel snow cover using MODIS observations. The Kaufman approach is essentially a variation of a "tie-point" algorithm using the 0.645-μm band (band 1) and the 2.1-μm band (band 7) of the MODIS instrument. The Barton method is a multivariate polynomial regression approach using the NDSI and MODIS observations.

While appreciating the strengths of other basic approaches such as multiple endmember spectral mixture analysis (Painter et al., 2003; Roberts et al., 1998) for getting better estimates of fractional snow cover within a pixel, there are attendant challenges and complexities of applying these or similar approaches on a daily, automated, global basis. Therefore, it was decided to examine whether the NDSI has enough of a "signal" to essentially extend the utility of the SNOWMAP approach to obtaining subpixel estimates of snow cover, retain the simplicity of the NDSI approach for doing automated, global mapping of snow cover, and offer advantages relative to other comparable methods (e.g., the Kaufman method and the Barton method) that nominally could be used to provide automated, global mapping of fractional snow cover.

## 3. Methods

To develop a relationship between NDSI and fractional snow cover within a MODIS 500-m pixel, it was necessary to utilize a source of ground truth. After considering the possibilities of utilizing aircraft and relatively high resolution satellite data, it was decided that the Enhanced Landsat Thematic Mapper-Plus (ETM+) observations would be readily available, suitable and effective. Several Landsat scenes covering a wide variety of snow-cover conditions were selected for study and subpixel snow-fraction algorithm development. These were: (a) a snow-covered region including glaciers in Alaska; (b) a relatively flat, snow-covered plains region in Labrador, Canada; (c) a taiga region in Siberia, Russia (Fig. 1). The specific dates and locations of these scenes are listed in Table 1. These scenes shown in Fig. 2 include diverse types of snow cover in different stages of accumulation and melting along with a reasonable amount of variety in attendant conditions of relief and land cover with which to develop a fractional snow-cover algorithm.


(a) Alaska


(b) Siberia, Russia


(c) Labrador, Canada

Fig. 1. Locations of the Landsat scenes that were used to develop fractional snow cover versus NDSI relationships. The box outlines the area covered by Landsat scenes shown in Fig. 2. (a) Alaska; (b) Siberia, Russia; (c) Labrador, Canada.

Table 1
Information about Landsat scenes used as ground truth in developing statistical relationships between fractional snow cover and NDSI and performing independent tests

| Region | Day | Path | Row | Sun elevation | Sun azimuth |
|---|---|---|---|---|---|
| Alaska | 05/12/01 | 065 | 017 | 46 | 162 |
| Siberia | 05/24/01 | 142 | 013 | 43 | 168 |
| Labrador | 11/07/00 | 11 | 020 | 15 | 168 |
| Kuparuk | 05/23/02 | 073 | 011 | 41 | 172 |
| South America | 12/08/01 | 232 | 084 | 58 | 077 |

In every Landsat scene used for the various regions indicated above, each 30-m pixel was classified as snow or non-snow using the current "SNOWMAP" approach to identify snow-covered pixels versus those not covered by snow (i.e., a binary classification). The Landsat ETM$^+$ bands (0.55-μm-band 2 and 1.64-μm band 5) corresponding to the MODIS bands 4 and 6 were used to calculate NDSI values.

MODIS and Landsat images collected on the same day with time separation of less than an hour were registered (Fig. 3) to a 500-m grid in a UTM projection. In each grid, an NDSI estimate based on MODIS observations of top-of-the-atmosphere reflectance in bands 4 and 6 was provided. Bilinear interpolation of reflectances was used to provide an NDSI value corresponding to a 500-m resolution grid cell center. For each 500-m grid cell, the percentage of snow cover was determined on the basis of the Landsat observations by counting the number of Landsat pixels covered by snow versus the total number of Landsat pixels in the cell.

Using the measures of snow fraction within 500-m cells as provided by Landsat, statistical linear relationships between the NDSI from MODIS observations and the true fraction of snow-cover from Landsat at 500-meter resolution were derived for three areas described above. A MODIS land/water mask was employed to exclude lakes, etc., from consideration to improve the statistical relationship between NDSI and true snow fraction. An ordinary least-squares regression approach was used to derive linear relationships between snow fraction (FRA) and NDSI corresponding to the 500-m grid cells.

Scatter plots of values for FRA versus the MODIS estimates of NDSI were examined for each of the three regions used in the study. Two different "models"/linear regressions were examined; namely, "model MA" expressed as $\mathrm{FRA} = a1 + b1 * \mathrm{NDSI}$ minimizing FRA deviations and "model MB" where $\mathrm{NDSI} = a2 + b2 * \mathrm{FRA}$ minimizes NDSI deviations. Examining the two relationships is relevant because it involves what is often termed the "errors-in-variables" problem (see Fuller, 1987; Lyon, 1970) and at least one other factor. Firstly, the fraction of snow-covered area (FRA)

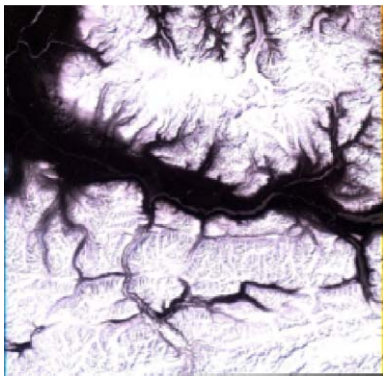

(a) Alaska, U.S.A

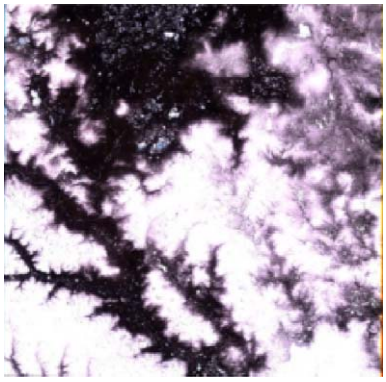

(b) Siberia, Russia

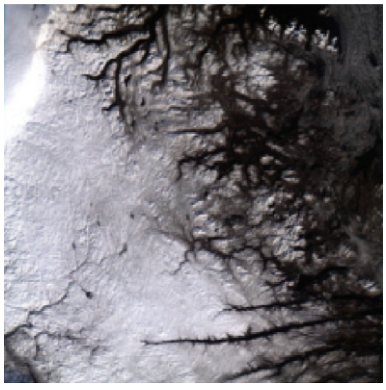

(c) Labrador, Canada

Fig. 2. Snow cover as imaged in Landsat scenes (see Table 1) used in providing ground-truth for the fractional snow-cover estimates from MODIS. (a) Alaska, USA; (b) Siberia, Russia; (c) Labrador, Canada.

derived from Landsat observations is better determined than the MODIS NDSI that has errors (as will be discussed later) related to variations in the reflectances used in the NDSI relationship caused by solar illumination and sensor view angles, snow grain size variability, and atmospheric effects. Given that situation, FRA nominally serves better as the independent variable and NDSI as the dependent variable. Secondly, a FRA on NDSI ordinary least squares (OLS) analysis minimizes the variance of FRA relative to the regression line extending for values of FRA above 1.0 and below 0.0 while an OLS analysis of NDSI on FRA inherently constrains the minimizing of NDSI variance over a range of FRA between 0.0 and 1.0. Based on these two factors, the MB model is more relevant except for the fact that the aim of the research being reported here is to estimate the FRA from the NDSI. To do that requires algebraically inverting the MB regression relationship to predict FRA from observed NDSI. This procedure is not unheard of (see Draper & Smith, 1981) and has been justified herein based on the factors just described. The model MB relationship gives a better visual fit to the data (see Fig. 4), and further tests to be described later show consistently better performance relative to the MA model as measured by mean absolute and rms error. A final

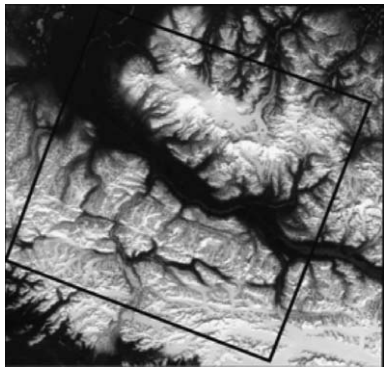

(a) Alaska, U.S.A.

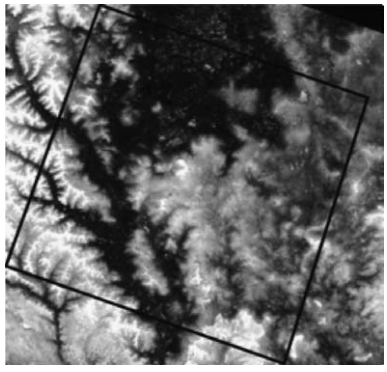

(b) Siberia, Russia

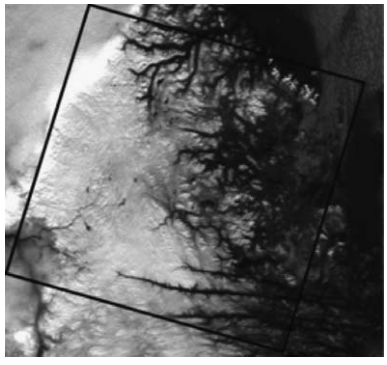

(c) Labrador, Canada

Fig. 3. Approximate location of Landsat scenes on companion MODIS scenes. Landsat and MODIS data were registered on a UTM grid. (a) Alaska, USA; (b) Siberia, Russia; (c) Labrador, Canada.

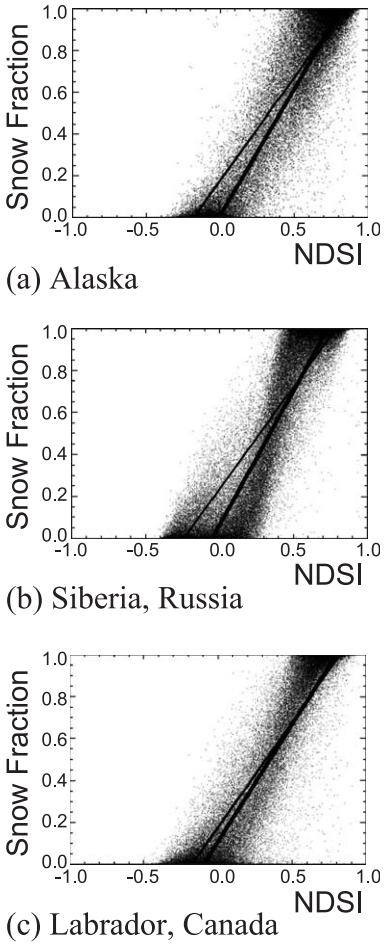


Fig. 4. Scatter plots of NDSI versus Fractional Snow cover (FRA) for the three test areas. The thin line is for relationship MA1. The thick line is for relationship MB3. (a) Alaska; (b) Siberia, Russia; (c) Labrador, Canada.

consideration in favor of the MB model was the steeper slope of the regression relationship providing more sensitivity of FRA to NDSI.

The performance of the models was examined when different criteria were employed in developing regression relationships. These different criteria were: (1) all the gridded MODIS NDSI values within the ground truth Landsat scenes were used whether the grid had any snow in it or not, (2) only grids with some snow (>0.0) were used, and (3) same as '2', but only for grids where the percentage of snow was >0.1. Table 2 lists the regression relationships for each of these conditions and Fig. 4 illustrates the relationships for the extremes in the conditions examined; i.e., model MA with criterion 1 (MA1) and model MB using criterion 3 (MB3).

## 4. Results

### 4.1. Tests of the models

As noted in the previous section examinations of the scatter plots, measures of error, and the relationships depicted indicate that the model MB3 performed best. The advantage of criterion 3 was simply that it eliminates the influence of non-snow-covered areas and situations where very little snow was observed. Once the MB3 model was selected, it was applied to all the data; i.e., there was no pre-screening of the observations for no snow or less than 0.1 snow fraction.

To test the stability and robustness of the MB3 model, two approaches were used. In one approach, the average relationship for two of the areas was obtained and then tested on the third area. For example, the averaged MB3 relationship for Siberia (S) [FRA = 0.06 + 1.28∗NDSI] and Labrador (L) [FRA = 0.11 + 1.12∗NDSI] was obtained (S + L) [FRA = 0.08 + 1.20∗NDSI] and tested on Alaska, etc. These results are shown in Table 3. In all of these instances, the relationships hold up quite well. Note, in particular, that the mean absolute error for the MB3 model (applied to all observations) produced a mean absolute error consistently well below 0.1 and a standard deviation very near to 0.1. This level of error includes effects due to variations in snow grain size, variability in the anisotropy of reflectance of snow and the effects of the atmosphere influencing the top-of-the-atmosphere reflectances used in the NDSI. In later paragraphs, an analysis of error was performed to assess the contribution of these factors and a comparison made to the mean absolute error and standard error levels shown in Tables 3 and 4.

Table 2
Regression relationships developed for each of the three test regions

| Subsets of pixels | Regions | Snow fraction (FRA) versus NDSI (model MA) | Snow fraction (FRA) versus NDSI (model MB) |
|---|---|---|---|
| All pixels (criteria 1) | | | |
| $n$ = 123,549 | Alaska | 0.17 + 0.99∗ NDSI | 0.14 + 1.05∗ NDSI |
| $n$ = 132,074 | Russia | 0.24 + 0.98∗ NDSI | 0.20 + 1.09∗ NDSI |
| $n$ = 83,379 | Labrador | 0.17 + 1.00∗ NDSI | 0.11 + 1.11∗ NDSI |
| Pixels with snow (criteria 2) | | | |
| $n$ = 108,108 | Alaska | 0.14 + 1.03∗ NDSI | 0.05 + 1.16∗ NDSI |
| $n$ = 108,376 | Russia | 0.17 + 1.08∗ NDSI | 0.09 + 1.25∗ NDSI |
| $n$ = 76,814 | Labrador | 0.17 + 1.00∗ NDSI | 0.11 + 1.11∗ NDSI |
| Pixels with FRA>0.1 (criteria 3) | | | |
| $n$ = 101,747 | Alaska | 0.19 + 0.97∗ NDSI | 0.00 + 1.22∗ NDSI |
| $n$ = 95,866 | Russia | 0.22 + 1.03∗ NDSI | 0.06 + 1.28∗ NDSI |
| $n$ = 66,398 | Labrador | 0.22 + 0.95∗ NDSI | 0.11 + 1.12∗ NDSI |

The number ($n$) of 500-m grid cells used to develop the regressions are shown for each area and criteria.

Table 3
Results showing the performance of the average relationship for Siberia and Labrador tested on Alaska, the average of Alaska and Siberia tested on Labrador, and the average relationship for Alaska and Labrador tested on Siberia

| Region | Mean snow cover | Version of model | Mean absolute error | rms error | Correlation coefficient |
|---|---|---|---|---|---|
| Alaska, $n=123,549$ | 0.73 | R+L | 0.04 | 0.09 | 0.98 |
| | | Alaska UB3 | 0.03 | 0.08 | 0.98 |
| Russia, $n=132,074$ | 0.56 | A+L | 0.08 | 0.13 | 0.97 |
| | | Russia UB3 | 0.06 | 0.11 | 0.97 |
| Labrador, $n=83,379$ | 0.64 | A+R | 0.06 | 0.11 | 0.96 |
| | | Labrador UB3 | 0.06 | 0.11 | 0.97 |

Another approach was to take the averaged MB3 result for all three areas and consider it to be the "universal" approach (MB3U). This relationship is:

$$\mathrm{FRA} = 0.06 + 1.21{*}\mathrm{NDSI}. \quad (2)$$

This MB3U relationship was then tested on two totally different areas; i.e., an independent/"blind" test was done. The new areas selected were (a) a mountainous region in the southern Andes of South America with an accompanying Landsat scene to provide the ground-truth and (b) a scene on the North Slope of Alaska covering the Kuparuk River Basin also having an accompanying Landsat scene. The locations of these two areas are shown in Fig. 5. At the same time, the performance of the fractional snow-cover algorithm developed in this paper was compared to the Kaufman et al. (2002) and Barton et al. (2001) methods. The Kaufman et al. relationship is:

$$\mathrm{FRA} = (\rho^{c}_{0.66} - 0.5\rho_{2.1})/\rho^{\mathrm{snow}}_{0.66}, \quad (3)$$

where $\rho^{c}_{0.66}$ is the corrected surface reflectance at 0.66 μm, $\rho_{2.1}$ is the reflectance at 2.1 μm, and $\rho^{0.66}_{\mathrm{snow}}$ is the reflectance of snow assumed to be equal to $0.6 \pm 0.1$.

Table 4
Results showing the various statistical comparisons between the best relationship developed in this paper (MB3U) and the relationships developed by Barton and Kaufman over areas independent where original relationships were developed

| Region | Method | Mean snow cover | Mean absolute error | rms error | Correlation coefficient |
|---|---|---|---|---|---|
| Kuparuk, $n=120,141$ | Barton | 0.33 | 0.14 | 0.19 | 0.93 |
| | Kaufman | 0.36 | 0.11 | 0.15 | 0.93 |
| | MB3U | 0.41 | 0.08 | 0.12 | 0.95 |
| South America, $n=135,234$ | Barton | 0.18 | 0.10 | 0.13 | 0.95 |
| | Kaufman | 0.22 | 0.07 | 0.10 | 0.96 |
| | MB3U | 0.21 | 0.04 | 0.10 | 0.97 |

The number of points involved in the testing of the MB3U is listed in the table.

(a) Alaska

(b) Chile/Argentina

Fig. 5. Square boxes indicate the location of test areas coincident with Landsat scenes in the North Slope of Alaska over the Kuparuk River Basin and in the Andes of Chile/Argentina used to test MB3 relationship for estimating fractional snow-cover area (FRA). (a) Alaska; (b) Chile/Argentina.

The Barton et al. relationship is:

$$\mathrm{FRA} = 0.18 + 0.37\mathrm{NDSI} + 0.26(\mathrm{NDSI})^2 + \ldots\ldots \quad (4)$$

Both Kaufman and Barton relationships were developed on a portion of the southern Sierra Nevada Mountains in the Southwestern United States. As such the tests of these relationships over the Andes and the Kuparuk river basin were also independent tests of these algorithms.

The results of the Andes and Kuparuk River basin test are shown in Fig. 6 and Table 4. In all cases, concurrent Landsat scenes were used to provide the ground truth for snow fraction (FRA) as described in Section 2 of this paper. In Table 4, it can be seen that MB3U relationship produced statistics that were generally better than the other two methods with the mean absolute error in particular showing some better performance.

To further evaluate the utility of the algorithm developed here, it was applied to a map of fractional snow cover over a large region covering most of the western United States. The results are compared to fractional snow-cover maps calculated using the Kaufman method and the Barton method as well as nearly concurrent maps of snow cover provided by

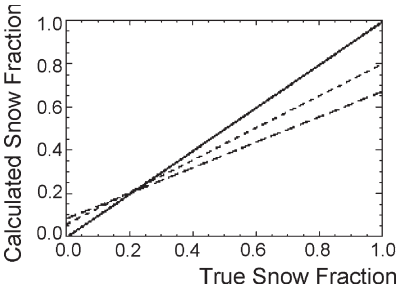


(a) Kuparuk River area

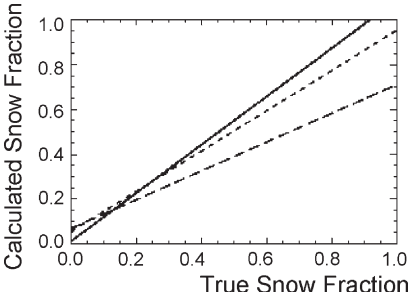


(b) South America Andes

Fig. 6. Regression lines for the calculated snow fraction (FRA) and the true snow fraction determined from Landsat approach (see Methods). The thick solid line is the result for MB3U, the line with the longer dashes is for the Barton method, and the line with the shorter dashes is for the Kaufman method. (a) Kuparuk River area; (b) South America Andes.

the NOHRSC (National Operational Hydrologic Remote Sensing Center)—see Carroll, 1995). These comparisons are shown in Fig. 7. These images show again that relative to the algorithm emphasized herein (MB3U), the Kaufman and Barton methods tend to overestimate snow-cover fraction at the low values (see small snow fractions over large regions where snow is not present) and underestimate snow cover where there is 100% or nearly 100% snow cover as, for example, should be expected at the top of mountain ranges.

### 4.2. Error analysis

As another examination of the performance of the MB3U algorithm, a rough error analysis was performed. One issue is the variability in the NDSI and subsequent estimates of FRA due to variability in snow grain size. Other factors were errors due to variability in the sensor view angle and the solar illumination of the snow (solar zenith angle) due to the anisotropy of snow reflectance. The fourth factor considered was the variability in the results for FRA and NDSI due to the effects of the "clear sky"/non-cloudy atmosphere on the top-of-the-atmosphere reflectances used in the NDSI For this analysis, results in the refereed literature were used to obtain a range in NDSI and FRA due to varying snow grain size, view or solar illumination angle, and atmospheric condition. Once having obtained the range, it was assumed that this was an approximation of $\pm 3\sigma$. From that approximation and the companion assumption that the errors were normally distributed, the standard deviation, $\sigma$, was computed for each of the factors considered. Then the root-mean-square (rms) of the four factors listed above was computed to give an estimate of total error that could then be compared to the regression mean absolute and standard error estimates.

In the case of the error due to snow grain size, Wiscombe and Warren (1980) observed that new snow has a 50-μm grain size, fine-grained older snow has a 200-μm grain size and old snow has a 1000-μm grain size. These grain sizes were used to approximate the $\pm 3\sigma$ is NSDI and FRA. In Wiscombe and Warren, graphs (their Fig. 8) of variability in albedo versus grain size are provided. Using this graph, albedo values for 0.55 μm (i.e., band 4 of MODIS) and 1.64 μm (band 6 of MODIS) were obtained for 50- and 1000-μm grain sizes and NDSI computed. These then were used in MB3U to obtain FRA. The end result was a standard deviation ($\sigma$) of 0.07. Other graphs of albedo versus grain size for different grain sizes were also examined; e.g., Aoki, Fukabori, and Uchiyama (1999) with similar, but usually somewhat smaller standard deviation results. To be conservative in the estimate of total rms error, the $\sigma = 0.07$ was retained.

As another way of examining the effect of grain size, MODIS observations of the megadunes in East Antarctica were analyzed (Fahnestock et al., 2000; Frezzotti et al., 2002). This is an area that is clearly 100% covered by snow and, although as yet not specifically characterized, some significant variability in grain size exists albeit the grain sizes are relatively large ( $\sim 1$ cm, see, http://nsidc.org/antarctica/megadune/dunes.html. "Megadunes: How the Dunes Were Formed). The dunes are spaced 2–5 km apart and have amplitudes of 2–4 m (Frezzotti, Gandolfi, & Urbini, 2002).

The NDSI was computed for MODIS 500-m pixels over the megadune area. The NDSI mean was 0.8 and the standard deviation of the observations was 0.02. This translates into a FRA of 1.0 and a standard deviation of 0.024. The standard deviation is somewhat lower than expected, but that is possibly due to the impact of variable grain size becoming increasingly limited at large grain sizes, the relative transparency of the atmosphere and uniformity of the terrain in this area. In any case, these observations do not suggest as much uncertainty in the FRA estimation due to grain size as the calculations in the previous corresponding paragraph indicate.

For the solar zenith angle factor, we utilized the results from Wiscombe and Warren (1980—Fig. 11a) over a range of solar zenith angles of 0–80°. Again it was assumed that this would provide an approximation of the $\pm 3\sigma$. The result was a standard deviation for FRA of 0.05. Although it is a rough (but conservative) estimate, we assumed the same standard deviation for sensor view angle—basically reflect-

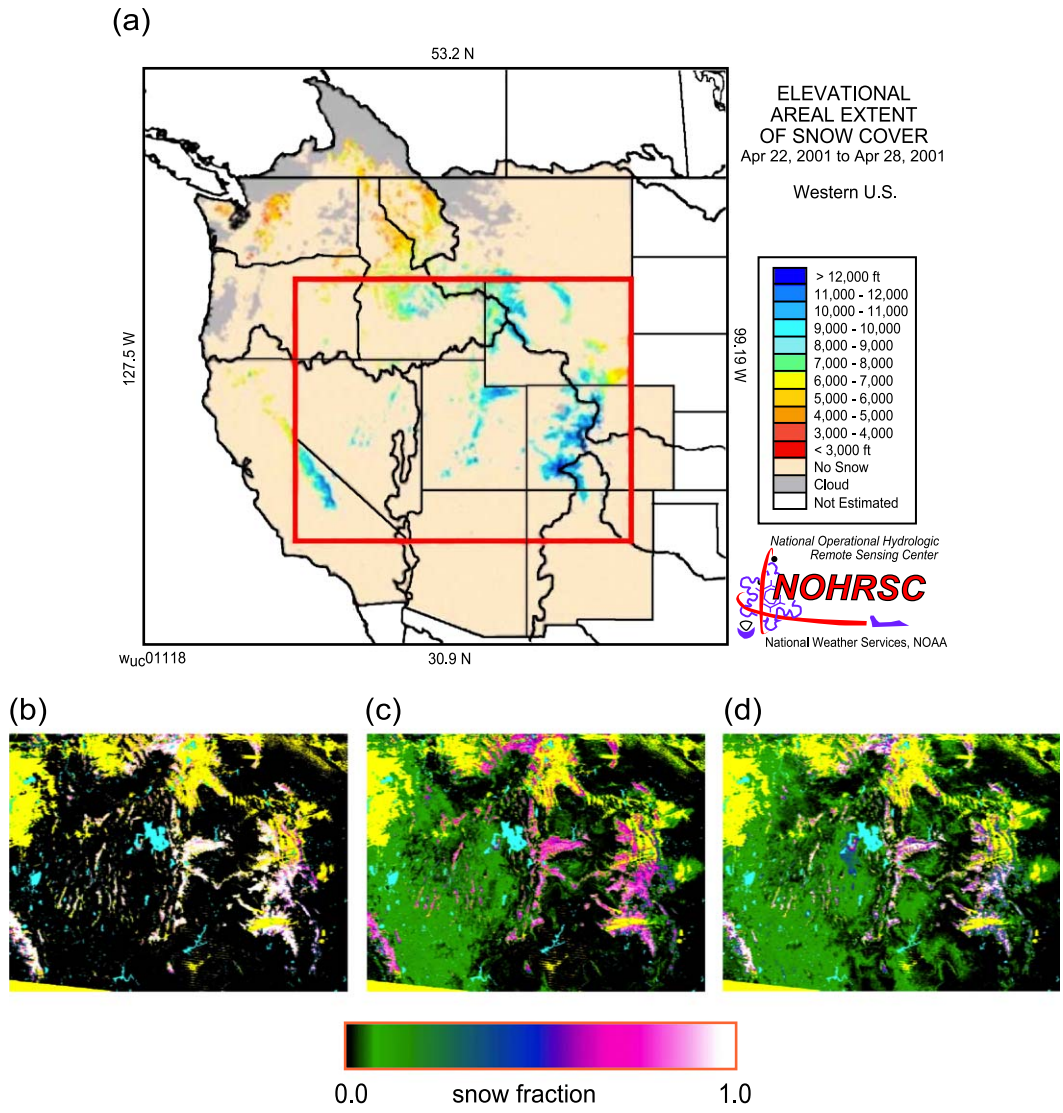


Fig. 7. Maps of snow cover over a large section of the western United States. The area covered in (b–d) is shown in the red box of panel a. Panel a is from the National Operational Hydrologic Remote Sensing Center (NOHRSC). Panel b shows fractional snow cover with the model MB3U developed in this paper. Panel c shows fractional snow cover as mapped by the Barton et al. (2001) algorithm. Panel d shows fractional snow cover as mapped by the Kaufman et al. (2002) algorithm. The yellow areas are those regions covered by clouds. The green areas, particularly in the lower left of (c) and (d), indicate erroneous estimates of low snow cover and the pink tones in (c) and (d) (see, for example, the fractional snow cover over the Uinta mountains in the center of the images) show the underestimate of snow cover by Kaufman and Barton techniques. In essence, the MB3U approach indicates more capability for capturing the total range in fractional snow cover.

ing the error associated with the anisotropy in the reflectance of snow.

For the atmospheric effect, we utilized the results in the work of Aoki et al. (1999—Fig. 10a) for an atmosphere with optical depth ranging from $\tau = 0.02-0.3$. The result was a standard deviation for FRA of 0.02.

Taking the square root of the sum of squares for all these factors (grain size, solar zenith angle, viewing angle, and atmospheric effect) the result was $[(0.07)^2+(0.05)^2+(0.05)^2+(0.02)^2]^{1/2}=[0.0049+0.0025+0.0025+0.0004]^{1/2}=[0.0103]^{1/2}=0.10$. This result corresponds closely to the rms and mean absolute error results already stated from the regression results.

## 5. Discussion

The results described above indicate that the fractional snow-cover algorithm discussed herein offers some improvements relative to other published fractional snow-cover algorithms published by Kaufman et al., and Barton et al. In the case of the Kaufman and Barton approaches versus the MB3 universal algorithm (MB3U) determined in this study, the MB3U approach generally does a better job of estimating snowfractions particularly at or near extremes; i.e., low snow fractions and high snow fractions while equaling or exceeding performance of these two methods in the mean as expressed by mean absolute error, rms error and correlations

coefficients. The results show that the mean absolute error for MB3U in independent tests (see Tables 3 and 4) stays at or below 0.10 and gives less rms error (Table 4). Overall, the MB3U approach appears to do a good job over a wide range of conditions while maintaining relative computational simplicity roughly equivalent to that of the existing SNOWMAP algorithm.

On the other hand, it should be noted that the approaches developed and applied here (e.g., MB3U) only give the fraction of snow that was observable in the MODIS pixel. That means, in particular, this algorithm makes no attempt to estimate snow beneath vegetation canopies such as those in forested areas as does the SNOWMAP approach (see Klein et al., 1998). As such the MB3U model is most useful in studies emphasizing the observing of fractional snow cover for its relationship to albedo and radiation balance research. It has limited utility for estimating snow cover in heavily forested areas and relating it to snowmelt runoff.

In addition, this study used radiances observed at the top of the atmosphere leading to the reflectances used in the NDSI. Studies are continuing to see if surface reflectances derived from MODIS observations and corrected for atmospheric effects (Vermote, El Saleous, & Justice, 2002) can improve upon the results. Furthermore, there may also be advantages yet undemonstrated or applied for MODIS observations to correct for viewing angle or bi-directional properties of snow in particular and other materials (see Schaaf et al., 2002) within a pixel and for topographic effects. Lastly, it is expected that this approach could be adjusted or "tuned" for specific areas such as watersheds or regions and subsequently increase the accuracy of the fractional snow-cover estimates.

## 6. Summary and conclusions

The normalized difference snow index (NDSI) has been examined to see if it provides sufficient "signal" to be useful in estimating fractional snow cover within a MODIS 500-m pixel. A globally applicable, linear statistical relationship has been developed using regions in Alaska, Canada and Russia. Tests in independent areas show that the relationship appears to be quite robust and stable. Comparisons are made to two other subpixel snow-cover algorithms applied to MODIS data showing that the fractional snow-cover relationship developed here provides better estimates especially for relatively low snow cover and high snow-cover conditions. The fraction of snow cover within a MODIS pixel can be provided with a mean absolute error of less than 0.1 over the entire range of 0.0–1.0.

## Acknowledgements

This work was supported by the NASA Earth Science Enterprise. Appreciation is expressed to Dr. Dorothy Hall and Dr. Yoram Kaufman for their reading of the manuscript and helpful suggestions. We also wish to thank Dr. Stephen Dery for his very helpful input regarding the use of fractional snow cover in models and Dr. Thomas Bell for discussions of errors in variables and other statistical data analysis issues.

## References

Aoki, T., Aoki, T., Fukabori, M., & Uchiyama, A. (1999). Numerical simulation of the atmospheric effects on snow albedo with a multiple scattering radiative transfer model for the atmosphere-snow system. *Journal of the Meteorological Society of Japan*, *77*, 595–614.

Barnes, W. L., Pagano, T. S., & Salomonson, V. V. (1998). Prelaunch characteristics of the moderate resolution imaging spectroradiometer (MODIS) on EOS-AM1. *IEEE Transactions on Geoscience and Remote Sensing*, *36*, 1088–1100.

Barton, J. S., Hall, D. K., & Riggs, G. A. (2001). Remote sensing of fractional snow cover using Moderate Resolution Imaging Spectroradiometer (MODIS) data. *Proceedings of the 57th Eastern Snow Conference, May 17–19, 2000, Syracuse, NY* (pp. 171–183).

Carroll, T. R. (1995). Remote sensing of snow in cold regions. *Proceedings of the First Moderate Resolution Imaging Spectroradiometer (MODIS) Snow and Ice Workshop, 13–14 September, 1995, Greenbelt, MD, NASA Conf. Pub., vol. 3318* (pp. 3–14).

Cess, R. D., Potter, G. L., Zhang, M. H., Blanchet, J. P., Chalita, S., Colman, R., Dazlich, D. A., Del Genio, A. D., Dymnikov, V., Galin, V., Jerrett, D., Keup, E., Lacis, A. A., Le Treut, H., Liang, X. Z., Mahfouf, J. F., Mcavaney, B. J., Melshko, V. P., Mitchell, J. F. B., Morcrett, J. J., Norris, P. M., Randall, D. A., Rikus, L., Roeckner, E., Royer, J. F., Schlese, U., Sheinin, D. A., Slingo, J. M., Sokolov, A. P., Taylor, K. E., Washington, W. M., Wetherald, R. T., & Yagai, I. (1991). Interpretation of snow-climate feedback as produced by 17 general circulation models. *Science*, *253*, 888–892.

Cohen, J. (1994). Snow and climate. *Weather*, *49*, 150–155.

Cohen, J., & Entekhabi, D. (2001). The influence of snow cover on Northern Hemisphere climate variability. *Atmosphere–Ocean*, *39*(1), 35–53.

Douville, H., & Royer, J. F. (1996). Sensitivity of the Asian summer monsoon to an anomalous Eurasian snow cover within the Meteo-France GCM. *Climate Dynamics*, *12*(7), 449–466.

Draper, N. R., & Smith, H. (1981). *Applied regression analysis* (pp. 47–51). New York, NY: Wiley.

Fahnestock, M. A., Scambos, T. A., Shuman, C. A., Arthern, R. J., Winebrenner, D. P., & Kwok, R. (2000). Snow megadune fields on the East Antarctic Plateau: Extreme atmospheric-ice interaction. *Geophysical Research Letters*, *27*, 3719–3722.

Foster, J., Liston, G., Koster, R., Essery, R., Behr, H., Dumenil, L., Verseghy, D., Thompson, S., Pollard, D., & Cohen, J. (1996). Snow cover and snow mass intercomparison of general circulation models and remotely sensed data sets. *Journal of Climate*, *9*, 409–426.

Frei, A., & Robinson, D. A. (1998). Evaluation of snow extent and its variability in atmospheric model intercomparison project. *Journal of Geophysical Research*, *103*, 8859–8871.

Frezzotti, M., Gandolfi, S., & Urbini, S. (2002). Snow megadunes in Antarctica: Sedimentary structure and genesis. *Journal of Geophysical Research*, *107*, 4344–4355.

Fuller, W. A. (1987). *Measurement error models* (pp. 30–59). New York, NY: Wiley.

Guenther, B., Xiong, X., Salomonson, V. V., Barnes, W. L., & Young, J. (2002). On-orbit performance of the Earth Observing System Moderate Resolution Imaging Spectroradiometer; first year of data. *Remote Sensing of Environment*, *83*, 16–30.

Hall, D. K., Riggs, G. A., & Salomonson, V. V. (1995). Development

of methods for mapping global snow cover using moderate resolution imaging spectroradiometer data. *Remote Sensing of Environment*, *54*(2), 127–140.

Hall, D. K., Riggs, G. A., Salomonson, V. V., DeGirolamo, N. E., Bayr, K. J., & Jin, J. M. (2002). MODIS Snow-cover products. *Remote Sensing of Environment*, *83*, 181–194.

Kaufman, Y. J., Kleidman, R. G., Hall, D. K., Martins, J. V., & Barton, J. S. (2002). Remote sensing of subpixel snow cover using 0.66 and 2.1 um channels. *Geophysical Research Letters*, *29*(16), 1781 (doi:10.1029. 2001GLO13580).

Klein, A. G., Hall, D. K., & Riggs, G. A. (1998). Improving snow-cover mapping in forests through the use of a canopy reflectance model. *Hydrological Processes*, *12*, 1723–1744.

Liston, G. E. (1995). Local advection of momentum, heat, and moisture during the melt of patchy snow covers. *Journal of Applied Meteorology*, *34*, 1705–1715.

Liston, G. E. (1999). Interrelationships among snow distribution, snowmelt, and snow cover depletion: Implications for atmospheric, hydrologic, and ecologic modeling. *Journal of Applied Meteorology*, *38*, 1474–1487.

Liston, G. E., Pielke Sr., R. A., & Greene, E. M. (1999). Improving first-order snow-related deficiencies in a regional climate model. *Journal of Geophysical Research*, *104*(16), 19559–19567.

Lyon, A. J. (1970). *Dealing with data* (pp. 263–264). New York, NY: Pergamon.

Nolin, A., & Liang, S. (2000). Progress in bidirectional reflectance modeling and applications for surface particulate media: Snow and soils. *Remote Sensing Reviews*, *14*, 307–342.

Nolin, A. W., Dozier, J., & Mertes, L. A. K. (1993). Mapping alpine snow using a spectral mixture modeling technique. *Annals of Glaciology*, *17*, 121–124.

Painter, T. H., Dozier, J., Roberts, D. A., Davis, R. E., & Green, R. O. (2003). Retrieval of subpixel snow-covered area and grain size from imaging spectrometer data. *Remote Sensing of Environment*, *85*, 64–77.

Rango, A., Walker, A. E., & Goodison, B. E. (2000). Role of snow and ice. In G. A. Schultz, & E. Engman (Eds.), *Remote sensing in hydrology and water management* (pp. 239–270). Berlin: Springer-Verlag.

Roberts, D. A., Gardner, M., Church, R., Ustin, S., Scheer, G., & Green, R. O. (1998). Mapping chaparral in the Santa Monica Mountains using multiple endmember spectral mixture models. *Remote Sensing of Environment*, *44*(2–3), 255–269.

Robinson, D. A., Dewey, K. F., & Heim, R. R. (1993). Global snow cover monitoring—an update. *Bulletin of the American Meteorological Society*, *74*(9), 1689–1696.

Roesch, A., Wild, M., Gilgen, H., Ohmura, A., & Arugnell, N. C. (2001). A new snow cover fraction parameterization for the ECHAM4 GCM. *Climate Dynamics*, *17*(2), 933–946.

Rosenthal, W., & Dozier, J. (1996). Automated mapping of montane snow-cover at subpixel resolution from the Landsat Thematic Mapper. *Water Resources Research*, *100*, 115–130.

Schaaf, C. B., Gao, F., Strahler, A. H., Lucht, W., Li, X., Tsang, T., Strugnell, N. C., Zhang, X., Jin, Y., Mueller, J., Lewis, P., Barnsley, M., Hobson, P., Disney, M., Roberts, G., Dunderdale, M., Doll, C., d'Entremont, R. P., Hu, B., Liang, S., Privette, J. L., & Roy, D. (2002). First operational BRDF, albedo nadir reflectance products from MODIS. *Remote Sensing of Environment*, *83*, 135–148.

Stieglitz, M., Ducharne, A., Koster, R., & Suarez, M. (2001). The impact of detailed snow physics on the simulation of snow cover and subsurface thermodynamics at continental scales. *Journal of Hydrometeorology*, *2*(3), 228–242.

Vermote, E. F., El Saleous, N. Z., & Justice, C. O. (2002). Atmospheric correction of MODIS data in the visible to middle infrared: First results. *Remote Sensing of Environment*, *83*, 97–111.

Vikhamer, D., & Solberg, R. (2002). Subpixel mapping of snow cover in forests by optical remote sensing. *Remote Sensing of Environment*, *84*, 69–82.

Wiscombe, W. J., & Warren, S. G. (1980). A model for the spectral albedo of snow. I: pure snow. *Journal of the Atmospheric Sciences*, *37*, 2712–2733.

Yang, Z. L., Dickinson, R. E., Hahmann, A. N., Niu, G. K., Shaikh, M., Gao, X. G., Bales, R. C., Sorooshian, S., & Jin, J. M. (1999). Simulation of snow mass and extent in general circulation models. *Hydrological Processes*, *13*(12–13), 2097–2113.